Design of Interior Permanent Magnet Synchronous Motor to Satisfy Given Output Characteristics in Lower or Higher Speed Operating Region

Yong-Sim Ro*

Faculty of Electrical Engineering, Kim Chaek University of Technology, 60-Kyogu, Yonggwang Street, Pyongyang, DPR Korea

***Corresponding Author**

DOI: https://dx.doi.org/10.47772/IJRISS.2025.909000436

Received: 24 August 2025; Accepted: 30 August 2025; Published: 14 October 2025

ABSTRACT

Satisfying the given output characteristics and achieving high efficiency in different operating speed regions are important in the optimal design of permanent magnet synchronous motors used as traction motors in urban electric vehicles.

In this paper, a method is proposed to determine the motor parameters that satisfy the given operating points in lower or higher speed operating region of output characteristics so that the motor performance can be kept in a high efficiency range.

The relationships between the motor operating points including maximum torque, base speed and maximum speed and design parameters including armature magnetic flux linkage, d-axis and q-axis inductance are considered. And the calculated expressions of relative motor parameters satisfying the operating characteristics such as the maximum torque in lower speed region and the maximum speed in higher speed region are derived.

This method was applied to the design of a 16 Nm interior permanent magnet synchronous motor (IPMSM) to verify that the design parameters satisfy the given output operating characteristics.

Keywords: IPMSM, motor parameter, output characteristics, high efficiency, operating point

INTRODUCTION

Permanent magnet synchronous motor (PMSM) is one of the essential actuation elements in modern machinery, including CNC machine tools and electric vehicles, and the accuracy of control and the quality of production depend on how it is designed.

Particularly traction motors used in urban electric vehicles require very high efficiency in operation, and hence, PMSM with low energy consumption is attractive. Therefore, minimizing energy losses is one of the most important criteria in the optimal design of PMSM [1, 2].

Traction motors for transport vehicles are required to work on the variable torque, power and speed profiles. Hence, it is necessary to evaluate the performance and the energy losses over the entire driving cycle with lower and higher speed regions, which is composed of different working points, and to design the optimum.

Some works designed to reduce the whole cycle into limited working points and minimize the energy consumption of the motor at some points [3]-[6].

The torque-speed and the power-speed characteristics of an electric vehicle can be represented by several curves. In the optimization of the design process in the literatures, the torque-speed characteristics are limited to several working points and the performance of the motor is evaluated by considering the equivalent weight factor at those points.

To reduce the computational time of energy loss over the whole cycle, the authors [7] proposed an analytical expression to determine copper loss and iron loss at every working point.

Here, copper and iron losses can be approximated as polynomial functions of d-axis and q-axis stator currents, which can be estimated from the torque-speed characteristics, reflecting the applied control algorithm. The coefficients of these polynomial functions can be determined using finite element simulations for some specified working points.

The above literatures proposed the methods to calculate the loss and efficiency of PMSM given in different torque-speed characteristics, but no method has been proposed to determine the design parameters suitable for torque-speed characteristics.

[8] presented a method for determining the pole pair number and stator diameter, design parameters of a high-speed permanent magnet synchronous motor for electric vehicles, such that the power density was maximized within a given driving cycle.

[9] and [11] determined the design parameters such as stator and rotor structure, air gap length, stator winding, slot number, etc. of high power density permanent magnet synchronous motor used as traction motor. [12] and [13] investigated the influence of diameter, length and turns per coil on the torque, power and efficiency of a permanent magnet synchronous machine on energy consumption in different drive cycles and different vehicle types.

However, to our knowledge, the design parameters that are important in determining the output characteristics of PMSM for electric vehicles are magnetic flux linkage, d- and q-axis inductance.

In [10], a design assist system was used to automatically determine the motor parameters that satisfy the demanded output characteristics as well as the required motor size. This design assist system was applied to the design of the surface permanent magnet synchronous motors and calculated the magnetic flux linkage and armature inductance for operating points of a given output characteristic.

In [14], a method was proposed for experimentally determining the design parameters of a model e.g., optimal current and magnetic flux linkage for torque control of a surface-mounted permanent magnet synchronous motor based on magnetic equivalent circuits. However, the above studies did not consider the variation of the d- and q-axis inductances because of the surface permanent magnet synchronous motor.

[15]-[20] proposed some methods to optimize the rotor core structure of surface and interior PMSM using a multi-objective optimization method including genetic algorithm. In particular, the d- and q-axis reluctances are

changeable depending on the rotor core structures in IPMSM. Literatures reported the principles to estimate design parameters mainly in binary space with respect to multi-objective functions, including current phase angle or material optimization, but they did not intend to determine parameters with reference to output characteristics.

The genetic algorithm and other optimization methods used so far have determined the structural parameters to maximize efficiency throughout the operation region, but the method of determining the structural parameters on the basis of the first determination of the characteristic parameters that satisfy the operating parameters under the conditions where the operating region where the efficiency is maximized is defined.

In this paper, we have studied the relationship between the torque-speed characteristics and the different parameters in PMSM, and suggested a method of determining the design parameters, including the magnetic flux linkage, the d- and q-axis inductance, to satisfy the torque-speed characteristics required for high efficiency. The proposed method was applied to the design of a 16 Nm IPMSM to get the parameters that satisfy the required mechanical characteristics.

This paper consists of 6 sections.

1. In Section 2, we presented the changeable range of current vectors to consider the variation of design parameters with the control strategy in PMSM.
2. Section 3 derives the relationship between the torque-speed and power-speed characteristics and the design parameters of PMSM.
3. Section 4 describes the method of determining the design parameters of the PMSM, expressed as relative parameters to satisfy a given output characteristic.
4. Section 5 presents the results of the design of the 16 Nm PMSM. Section 6 concludes the paper.

Current vector change for permanent magnet synchronous motors

Generally, the current control is mostly vector control, and the optimal current vector control is applied to PMSM to obtain the maximum output under the different control strategies.

The most common mathematical model for analysing PMSM is considered in the d-q reference frame, which is used to analyse the steady-state and transient operating conditions of PMSM.

Fig. 1 shows the model of PMSM.

The stator voltage equation of the PMSM in stationary reference frame is written as

$$\begin{bmatrix} u_u \\ u_v \\ u_w \end{bmatrix} = R_a \begin{bmatrix} i_u \\ i_v \\ i_w \end{bmatrix} + \frac{d}{dt} \begin{bmatrix} \psi_u \\ \psi_v \\ \psi_w \end{bmatrix} \quad (1)$$

Fig. 1. Model of permanent magnet synchronous motor

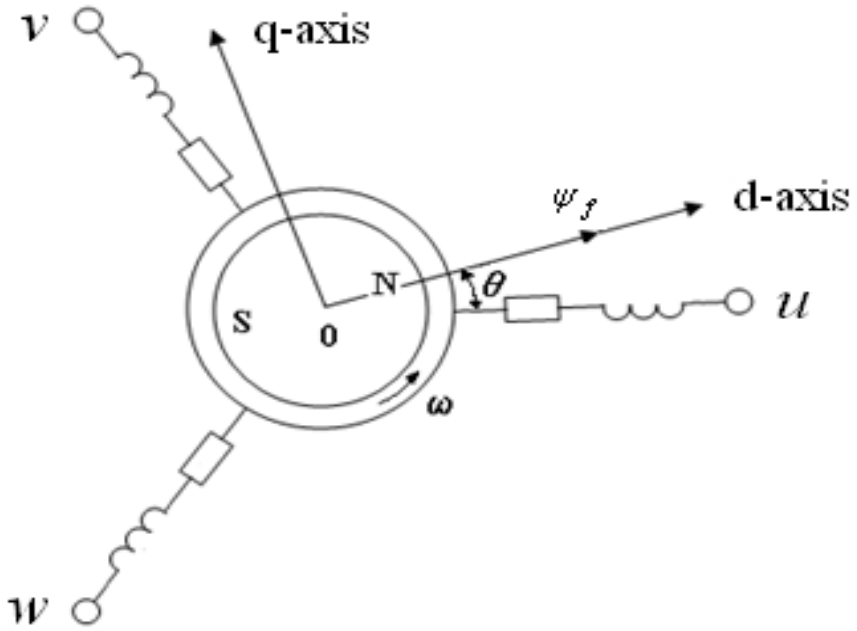

These are converted into the direct voltages in the rotating reference frame with angular velocity ω, and the voltage and flux linkage equations are expressed as follows.

$$\begin{cases} u_d = R_a i_d + \dfrac{d\psi_d}{dt} - \omega\psi_q \\ u_q = R_a i_q + \dfrac{d\psi_q}{dt} - \omega\psi_d \end{cases} \quad (2)$$

$$\begin{cases} \psi_d = L_d i_d + \psi_f \\ \psi_q = L_q i_q \end{cases} \quad (3)$$

where u_d and u_q are the d-q axis stator voltages, i_d and i_q are the d-q axis stator currents, R_a is the armature phase resistance, ψ_d and ψ_q are the d-q axis magnetic flux linkages, ω is the electrical angular speed, L_d and L_q are the d-q axis inductances, and ψ_f is the rotor permanent magnet flux linkage.

Considering the current and voltage limitations, we can express the armature current, the induced voltage and magnetic flux linkage as follows:

$$I_a = \sqrt{i_d^2 + i_q^2} \le I_{am} \quad (4)$$

$$V_o = \omega\sqrt{\left(L_d I_d + \psi_f\right)^2 + \left(L_q I_q\right)^2} \leqq V_{om} \quad (5)$$

$$\psi_o = \sqrt{\psi_d^2 + \psi_q^2} = \sqrt{\left(L_d I_d + \psi_f\right)^2 + \left(L_q I_q\right)^2} \quad (6)$$

The armature current limit I_{am} corresponds to the rated current of the motor in continuous operation and the induced voltage limit V_{om} corresponds to the maximum value of the inverter output voltage.

The current limit of (4) and the voltage limit of (5) are plotted in plane as shown in Fig. 2.

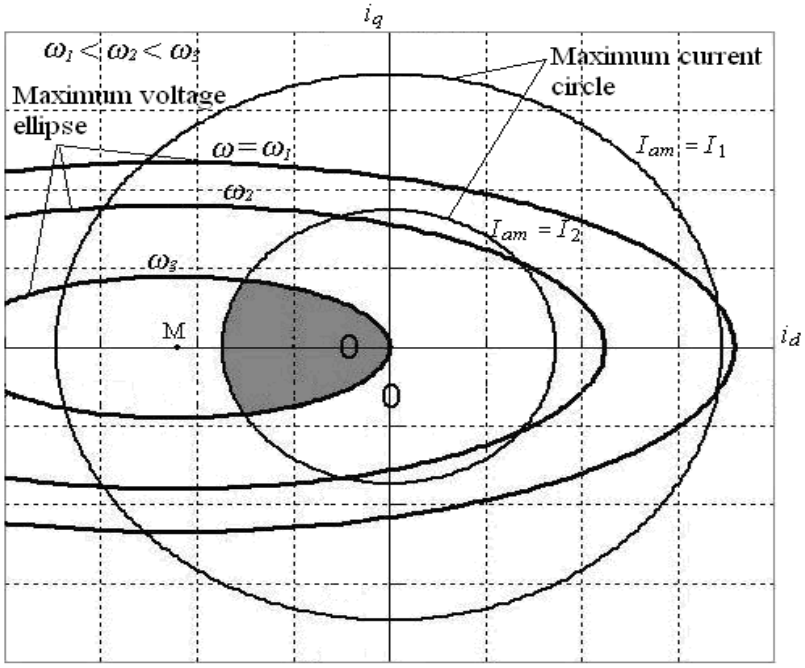

The current is limited to the inner region of the maximum current circle, expressed in Eq. (4), and the voltage is limited to the inner region of the maximum voltage ellipse, expressed in Eq. (5). The current vector to satisfy both current and voltage limits is being in the inner region (dark coloured) of the maximum current circle and the maximum voltage ellipse.

The maximum voltage ellipse decreases to approach point M $\left(i_d = -\psi_f / L_d,\ i_q = 0\right)$ with increasing speed even though the voltage limit is constant. Depending on whether the point M is inside or outside the maximum current circle, the control method or the output characteristic of the PMSM in the high-speed region will be changed.

If the point M is inside the maximum current circle, i.e., $\psi_f < L_d I_{am}$, the current vectors are available for the speed to be infinite theoretically. If the point M is outside the maximum current circle, i.e., $\psi_f > L_d I_{am}$, on the contrary, the maximum current circle and the maximum voltage ellipse are separated above a certain speed and the current vector becomes not available which is the limit of operation.

When the induced voltage due to the permanent magnets reaches the voltage limit, the angular speed is called base speed given as follows:

$$\omega_{base} = \frac{V_{om}}{\psi_o} \tag{7}$$

The maximum voltage ellipse at the base speed is tangent to the origin. In order to operate at speeds above the base speed, it is always necessary for the d-axis current to be negative even at no load.

Torque-Speed characteristics of permanent magnet synchronous motor

Suppose that the PMSM is controlled by the maximum torque per current ratio control method.

In lower speed operation than the reference speed, the voltage does not reach the limiting value and only the current limitation is considered.

The torque of the PMSM is expressed as (8), the first term is the torque due to the permanent magnet and the second term is the reaction torque.

$$T = p(\psi_d I_q - \psi_q I_d) = p\left[\psi_f I_q + (L_d - L_q) I_d I_q\right] \quad (8)$$

Now consider the relationship between I_d and I_q to maximize this torque.

If the current vector leads q-axis reference current by the angle β, $I_d = -I_a \sin\beta$, $I_q = I_a \cos\beta$, and Eq. (8) is transformed into

$$\begin{aligned} T &= p\left[\psi_f I_a \cos\beta + (L_q - L_d)\cdot I_a \sin\beta \cdot I_a \cos\beta\right] = \\ &= p\left[\psi_f I_a \cos\beta + \frac{1}{2}(L_q - L_d)\cdot I_a^2 \sin 2\beta\right] \end{aligned} \quad (9)$$

Since the $T = f(\beta)$ of Eq. (9) is a convex function, Eq. (9) is differentiable with respect to β, and the right side of the differential equation is set to zero to get the maximum torque value as follows:

$$\frac{\partial T}{\partial \beta} = p\left[\psi_f I_a \cdot (-\sin\beta) + (L_q - L_d)\cdot I_a^2 \cos 2\beta\right] = 0 \quad (10)$$

The value of β at which the torque is maximized: $\beta = \arcsin \dfrac{-\psi_f + \sqrt{\psi_f^2 + 8(L_q - L_d)^2 I_a^2}}{4(L_q - L_d) I_a}$ (11)

Substituting β from Eq. (11) the d-axis current I_{d1}, q-axis current I_{q1} are expressed as follows:

$$I_{d1} = \frac{\psi_f}{4(L_q - L_d)} - \sqrt{\frac{\psi_f^2}{16(L_q - L_d)^2} + \frac{I_{am}^2}{2}} \quad (12)$$

$$I_{q1} = \sqrt{I_{am}^2 - I_{d1}^2} \quad (13)$$

The torque is maximum as $I_a = I_{am}$, and the operating point is the intersection point A of the maximum torque/current curve and the maximum current circle as shown in Fig. 3, the d and q-axis currents are expressed by Eq. (12) and (13), and the armature flux linkage is

$$\psi_0 = \sqrt{\left(\psi_f + L_d I_{d1}\right)^2 + \left(L_q I_{q1}\right)^2} \tag{14}$$

As the induced voltage $V_o\left(=\omega\psi_0\right)$ reaches the limited value V_{om}, the angular speed of rotation is

$$\omega_{\text{base}} = \frac{V_{om}}{\psi_0} = \frac{V_{om}}{\sqrt{\left(\psi_f + L_d I_{d1}\right)^2 + \left(L_q I_{q1}\right)^2}} \tag{15}$$

The maximum voltage ellipse intersects point A at this speed, and at higher speeds, the current vector cannot be controlled at point A. Therefore the rated operation is ranged from zero speed to reference speed ω_{base} while operating at maximum torque. In this operation region, the current $I_a = I_{am}$, and the voltage $V_o < V_{om}$.

Operating above the reference speed, the voltage limitation is considered.

To maximize the torque in this region, the current vector is controlled toward the intersection point B of the maximum current circle and the maximum voltage ellipse, at which the current $I_a = I_{am}$ and the voltage $V_0 = V_{om}$.

Considering the current and the armature flux linkage,

$$\begin{cases} \sqrt{I_d{}^2 + I_q{}^2} = I_{am} \\ \psi_0 = \sqrt{\left(\psi_f + L_d I_{d1}\right)^2 + \left(L_q I_{q1}\right)^2} = \dfrac{V_{om}}{\omega} \end{cases} \tag{16}$$

At the point B from Fig. 3, the d-axis current is denoted by I_{d2} and the q-axis current I_{q2}, expressed as follows:

$$I_{d2} = \frac{\psi_f L_d - \sqrt{\left(\psi_f L_q\right)^2 + \left(L_q^2 - L_d^2\right)\left\{\left(L_q I_{am}\right)^2 - \left(\dfrac{V_{om}}{\omega}\right)^2\right\}}}{L_q^2 - L_d^2} \tag{17}$$

$$I_{q2} = \sqrt{I_{am}^2 - I_d^2} \tag{18}$$

Increasing the speed continuously, the operating point gradually moves from point B to point D.

If the minimum value of d-axis flux linkage $\psi_{d\min} = \psi_f - L_d I_{am}$ < 0, the current vector then moves on the maximum torque / flux curve to point M as the speed increases, as shown in Fig 3 (a), while the current $I_a = I_{am}$

and the voltage $V_o < V_{om}$.

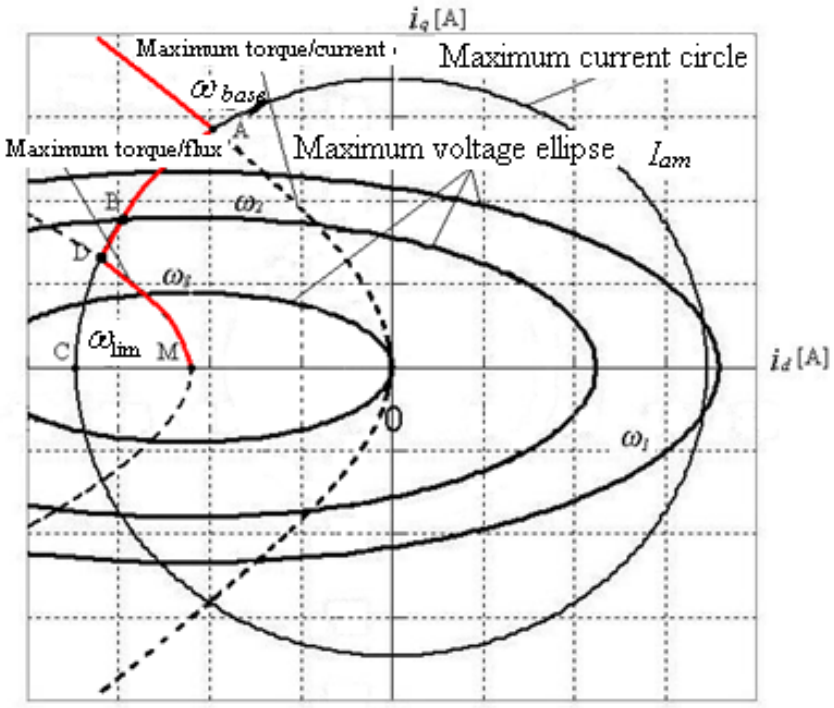

(a) $\psi_{dmin} = \psi_f - L_d I_{am} < 0$

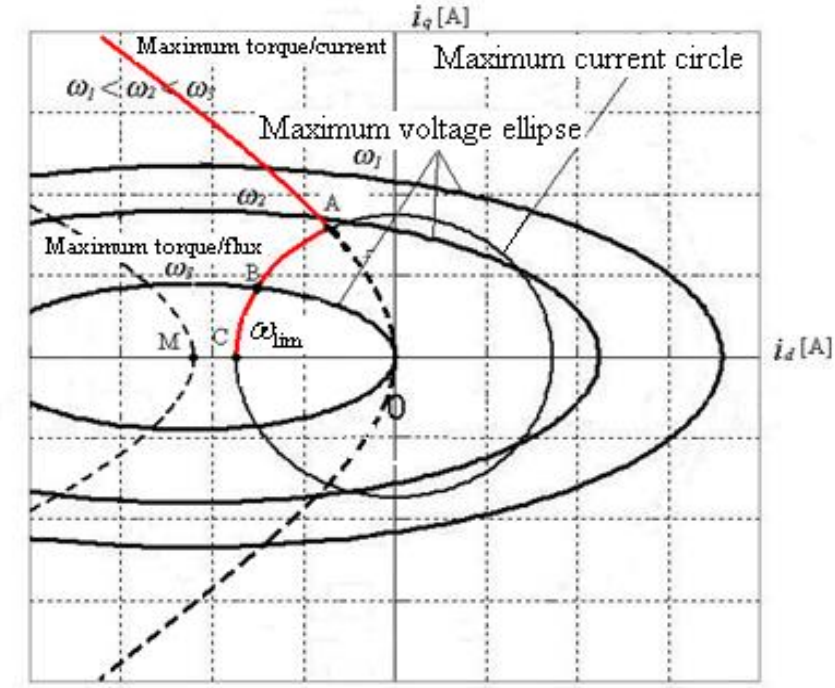

(b) $\psi_{dmin} = \psi_f - L_d I_{am} > 0$

Fig. 3. Current vector trajectory with increasing speed of constant torque control

Here the voltage limitation is only considered, and the maximum torque/flux control is applied to get the maximum output power.

The d-axis current is denoted as I_{d3}, and the q-axis current I_{q3}, in this region, expressed as follows:

$$I_{d3} = -\frac{\psi_f + \Delta\psi_d}{L_d} \tag{19}$$

$$I_{q3} = \frac{\sqrt{\left(\frac{V_{om}}{\omega}\right)^2 - (\Delta\psi_d)^2}}{L_q} \tag{20}$$

where

$$\Delta\psi_d = \frac{-L_q\psi_f + \sqrt{(L_q\psi_f)^2 + 8(L_q - L_d)^2\left(\frac{V_{om}}{\omega}\right)^2}}{4(L_q - L_d)} \tag{21}$$

However, if the minimum value of d-axis flux linkage $\psi_{d\min} = \psi_f - L_d I_{am} > 0$, the maximum torque/flux control is impossible to be applied, because the maximum torque/flux curve (maximum power/voltage curve) is being outside the maximum current circle at the speed over ω_d, the speed at the point D. Here the current and the voltage are expressed as (17) and (18) respectively.

At the speed the maximum voltage ellipse is tangent to the maximum current circle, the current vector reaches the point C ($I_d = -I_{am}$, $I_q = 0$), as shown in Fig 3 (b), and the power is to be zero.

This speed is just the power limit speed expressed as follows:

$$\omega_{\lim} = \frac{V_{om}}{\psi_f - L_d I_{am}} = \frac{V_{om}}{\psi_{d\min}} \tag{22}$$

where $\psi_{d\min} = \psi_f - L_d I_{am}$

$\psi_{d\min}$ is the minimum value of d-axis flux linkage as a result of the maximum flux-reducing MMF, which is an important parameter to determine the range of the high-speed constant power operation.

Substituting the different expressions for I_d and I_q induced above for the different operation ranges into Eq. (8), and considering the power as the product of torque by angular speed, we can get the torque-speed characteristics and the power-speed characteristics as shown in Fig. 4.

Fig. 4. Torque-Speed characteristics and Power-Speed characteristics

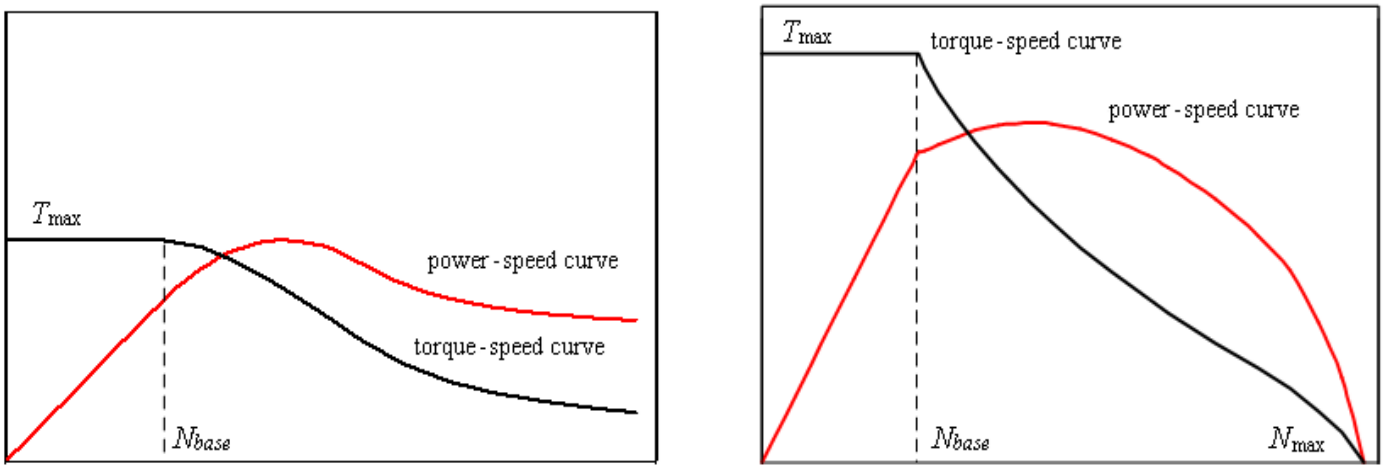

(a) $\psi_{dmin} = \psi_f - L_d I_{am} < 0$ (b) $\psi_{dmin} = \psi_f - L_d I_{am} > 0$

As shown in the figure, there is a close relationship between the design parameters and characteristics of the PMSM.

ψ_{dmin} decides the possible operation range over the reference speed.

If $\psi_{dmin} = \psi_f - L_d I_{am}$, the minimum value of the d-axis flux linkage, is less than 0, then the maximum possible torque at the reference speed gets smaller, but the maximum speed gets larger, and vice versa.

Therefore, it is desirable to determine the design parameters of the PMSM to satisfy the given output characteristics, including maximum torque and maximum speed.

Determination of design parameters of permanent magnet synchronous motor by torque-speed characteristics

Since the torque-speed characteristics of PMSM differ from one motor to another, to generalize them, let us consider the design parameters as relative values.

Using the armature current limit I_{am}, the induced voltage limit V_{om} and the base speed ω_{base}, the armature current, induced voltage, angular speed, output power, torque, armature resistance, flux linkage and inductance can be expressed by the relative value as follows :

$$I^*_a = \frac{I_a}{I_{am}},\ V^*_o = \frac{V_o}{V_{om}},\ \omega^* = \frac{\omega}{\omega_{\text{base}}},\ P^* = \frac{P}{V_{om} I_{am}},$$
$$T^* = \frac{T\omega_{\text{base}}}{V_{om} I_{am}},\ R^* = \frac{R I_{am}}{V_{om}},\ \psi^* = \frac{\omega_{\text{base}}\psi}{V_{om}},\ L^* = \frac{\omega_{\text{base}} L I_{am}}{V_{om}} \quad (23)$$

Considering $I^*_{am}=1$ and $V^*_{om}=1$, we can neglect the armature resistance and generalize the relationship between the design parameters and the output characteristics.

In the maximum torque per ampere control region operating under the base speed, the voltage is less than the voltage limit and the optimal current vector should be on the maximum current circle, i.e. $I_a=I_{am}$, $V_o<V_{om}$ .The generalized currents of the d- and q-axis currents to get the maximum torque can be written as

$$I^*_{d1}=\frac{\psi^*_f}{4\left(L^*_q-L^*_d\right)}-\sqrt{\frac{{\psi^*_f}^2}{16\left(L^*_q-L^*_d\right)^2}+\frac{1}{2}} \tag{24}$$

$$I^*_{q1}=\sqrt{{I^*_{am}}^2-{I^*_{d1}}^2}=\sqrt{1-{I^*_{d1}}^2} \tag{25}$$

The maximum torque expressed by the relative value is

$$\begin{aligned}T^*_{\max}&=\frac{p\left[\psi_f I_{q1}+\left(L_d-L_q\right)I_{d1}I_{q1}\right]}{V_{om}I_{am}}\omega_{\text{base}}\\&=p\left[\psi^*_f\cdot I^*_{q1}+\left(L^*_d-L^*_q\right)\cdot I^*_{d1}\cdot I^*_{q1}\right]\\&=p\left\{\psi^*_f\cdot\sqrt{\frac{\psi^*_f}{2\left(L^*_d-L^*_q\right)}\left[\sqrt{\frac{{\psi^*_f}^2}{16\left(L^*_d-L^*_q\right)^2}+\frac{1}{2}}-\frac{\psi^*_f}{4\left(L^*_d-L^*_q\right)}\right]}-\frac{1}{2}+\right.\\&\quad+\left(L^*_d-L^*_q\right)\cdot\left[\frac{\psi^*_f}{4\left(L^*_d-L^*_q\right)}-\sqrt{\frac{{\psi^*_f}^2}{16\left(L^*_d-L^*_q\right)^2}+\frac{1}{2}}\right]\times\\&\quad\left.\times\sqrt{\frac{\psi^*_f}{2\left(L^*_d-L^*_q\right)}\left[\sqrt{\frac{{\psi^*_f}^2}{16\left(L^*_d-L^*_q\right)^2}+\frac{1}{2}}-\frac{\psi^*_f}{4\left(L^*_d-L^*_q\right)}\right]}-\frac{1}{2}\right\}\end{aligned} \tag{26}$$

If $\omega=\omega_{\text{base}}$, i.e. $\omega^*=\omega^*_{\text{base}}=1$ from Eq. (23), then $V_o=V_{om}$, i.e. $V^*_o=1$ and Eq. (14) can be written as

$$\psi^*_0=\sqrt{\left(\psi^*_f+L^*_dI^*_d\right)^2+\left(L^*_qI^*_q\right)^2}=1 \tag{27}$$

Substitute Eq. (24) and (25) into Eq. (27), because it can be also satisfied with I^*_{d1} and I^*_{q1}.

$$\begin{aligned}&\left(\psi^*_f+L^*_dI^*_{d1}\right)^2+\left(L^*_qI^*_{q1}\right)^2={\psi^*_f}^2+{L^*_d}^2+\left({L^*_q}^2-{L^*_d}^2\right){I^*_{q1}}^2+2\psi^*_fL^*_dI^*_{d1}=\\&={\psi^*_f}^2+\frac{\psi^*_f\left(5L^*_d+L^*_q\right)}{2}\left[\frac{\psi^*_f}{4\left(L^*_d-L^*_q\right)}-\sqrt{\frac{{\psi^*_f}^2}{16\left(L^*_d-L^*_q\right)^2}+\frac{1}{2}}\right]+\frac{\left(3{L^*_d}^2-{L^*_q}^2\right)}{2}=1\end{aligned} \tag{28}$$

From Eq. (28), the three motor parameters Ψ^*_f, L^*_d and L^*_q can be formed a curved surface as shown in Fig. 5.

Fig. 5. Possible range of three motor parameters of PMSM

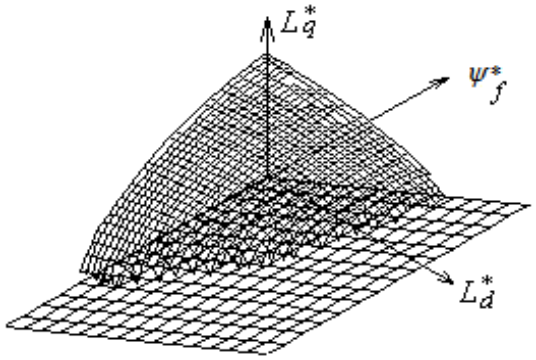

In the flux-weakening control region operating above the base speed, the current vector should be controlled by the intersection of the maximum current circle and the maximum voltage ellipse. In this region, the current and induced voltage are always $I_a = I_{am}$, $V_o = V_{om}$ and the d- and q-axis currents expressed by the relative values can be written as

$$I^*_{d2} = \frac{\psi^*_f L^*_d - \sqrt{\left(\psi^*_f L^*_q\right)^2 + \left(L^{*2}_q - L^{*2}_d\right)\left[\left(L^*_q\right)^2 - \left(\frac{1}{\omega^*}\right)^2\right]}}{L^{*2}_q - L^{*2}_d} \tag{29}$$

$$I^*_{q2} = \sqrt{1 - I^{*2}_{d2}} \tag{30}$$

As the speed continues to rise, the current vector enters into the maximum voltage ellipse. If $\psi_{d\min} = \psi_f - L_d I_{am}$ <0, the current vector is moved by maximum torque per voltage control to the point M in Fig. 1. In this region, the current and voltage are $I_a < I_{am}$, $V_o = V_{om}$. Here the d- and q-axis current to obtain the maximum torque per voltage are expressed as

$$I^*_{d3} = -\frac{\psi^*_f + \Delta\psi^*}{L^*_d} \tag{31}$$

$$I^*_{q3} = \frac{\sqrt{\left(\frac{1}{\omega^*}\right)^2 - \left(\Delta\psi^*\right)^2}}{L^*_q} \tag{32}$$

where

$$\Delta\psi^* = \frac{-L^*_q\psi^*_f + \sqrt{\left(L^*_q\psi^*_f\right)^2 + 8\left(L^*_q - L^*_d\right)^2\left(\frac{1}{\omega^*}\right)^2}}{4\left(L^*_q - L^*_d\right)} \tag{33}$$

If $\psi_{dmin} = \psi_f - L_d I_{am} > 0$, the point M is outside the maximum current circle and the maximum torque per voltage control is impossible. In this region, the current vector finally reaches the point where $I_d = -I_{am}$, $I_q = 0$ at the maximum, and the output power is zero.

This maximum speed is the power limit speed and its relative value can be written as

$$\omega^*_{\max} = \frac{V^*_{om}}{\psi^*_f - L^*_d I^*_{am}} = \frac{1}{\psi^*_f - L^*_d} \tag{34}$$

Generally, the maximum torque, maximum speed, base speed, maximum current and voltage are given from the demanded operating points on output characteristics.

From Eq. (26), (28) and (34), the simultaneous equations with the relative parameters ψ^*_f, L^*_d and L^*_q are written as follows:

$$\begin{cases} P\left\{\psi^*_f \cdot \sqrt{\frac{\psi^*_f}{2(L^*_d - L^*_q)}\left[\sqrt{\frac{\psi^{*2}_f}{16(L^*_d - L^*_q)^2} + \frac{1}{2}} - \frac{\psi^*_f}{4(L^*_d - L^*_q)}\right]} - \frac{1}{2} + \right. \\ + (L^*_d - L^*_q)\cdot\left[\frac{\psi^*_f}{4(L^*_d - L^*_q)} - \sqrt{\frac{\psi^{*2}_f}{16(L^*_d - L^*_q)^2} + \frac{1}{2}}\right] \times \\ \left. \times \sqrt{\frac{\psi^*_f}{2(L^*_d - L^*_q)}\left[\sqrt{\frac{\psi^{*2}_f}{16(L^*_d - L^*_q)^2} + \frac{1}{2}} - \frac{\psi^*_f}{4(L^*_d - L^*_q)}\right]} - \frac{1}{2}\right\} = \frac{T_{\max}\omega_{base}}{V_{om} I_{am}} \\ \frac{1}{\psi^*_f - L^*_d} = \frac{\omega_{\max}}{\omega_{base}} \\ \psi^{*2}_f + \frac{\psi^*_f (5L^*_d + L^*_q)}{2}\left[\frac{\psi^*_f}{4(L^*_d - L^*_q)} - \sqrt{\frac{\psi^{*2}_f}{16(L^*_d - L^*_q)^2} + \frac{1}{2}}\right] + \frac{(3L^{*2}_d - L^{*2}_q)}{2} = 1 \end{cases} \tag{35}$$

Solve the above equations and three relative parameters can be calculated. Then the real motor parameters are transformed as follows:

$$L_d = \frac{V_{om} L^*_d}{\omega_{base} I_{am}} \tag{36}$$

$$L_q = \frac{V_{om} L^*_q}{\omega_{base} I_{am}} \tag{37}$$

$$\psi_f = \frac{V_{om} \psi^*_f}{\omega_{base}} \tag{38}$$

The two-dimensional curve of Fig. 5 with the coordinates of L^*_d and L^*_q is shown in Fig. 6.

Here, the family of curves is the one with varying ψ_f^*, and their detailed calculations are given in Table 1.

Fig. 6. Two-dimensional curve for parameter design of PMSM

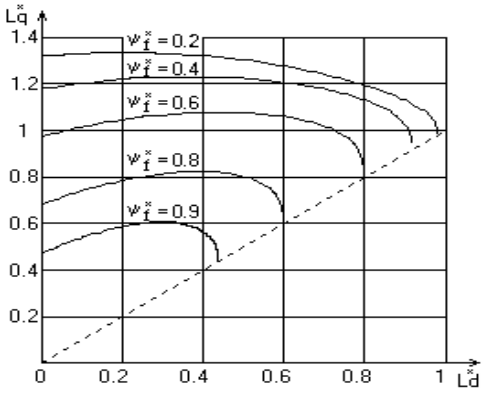

Table 1. Some of relative parameters of PMSM

№	ψ_f^*	L_q^*		
		L_d^* =0.3	L_d^* =0.4	L_d^* =0.5
1	0.2	1.33	1.32	1.3
2	0.4	1.23	1.23	1.215
3	0.6	1.065	1.075	1.085
4	0.8	0.815	0.82	0.83
5	0.9	0.605	0.61	0.62

The dotted line in Fig. 6 represents the non-salient motor, and its upper left region represents the salient motor. We can get the different torque-speed characteristics of the PMSM according to the calculated results in Table 1.

Examples

A 16Nm IPMSM was designed to satisfy the given torque-speed characteristic.

The specifications of the IPMSM are listed in Table 2, and the given torque-speed characteristic is shown in Fig 7.

Table 2. Spécifications of the IPMSM

Item (Unit)	Value
Maximum torque T_{max} (Nm)	16
Armature current limit I_{am} (A)	28

Induced voltage limit V_{om} (V)	72
Base speed N_{base} (min^{-1})	1200
Power limit speed N_{max} (min^{-1})	3000
Number of poles 2p	6

Fig. 7. Given output characteristic

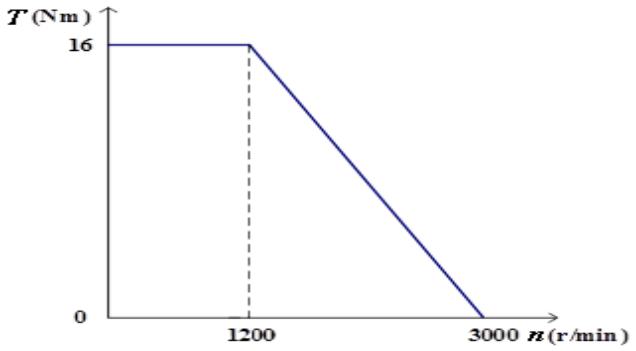

A flowchart for the proposed calculation of motor parameters to satisfy the output characteristic is shown in Fig. 8. The relative motor parameters are obtained from the demanded torque-speed characteristic, and the calculated output characteristic can be drawn from the motor parameters as shown in Fig. 9. The calculated maximum torque is 16.01Nm as shown in Fig. 9, with a relative error of about 0.63%.

Fig. 8. Flowchart for motor parameter calculation of PMSM

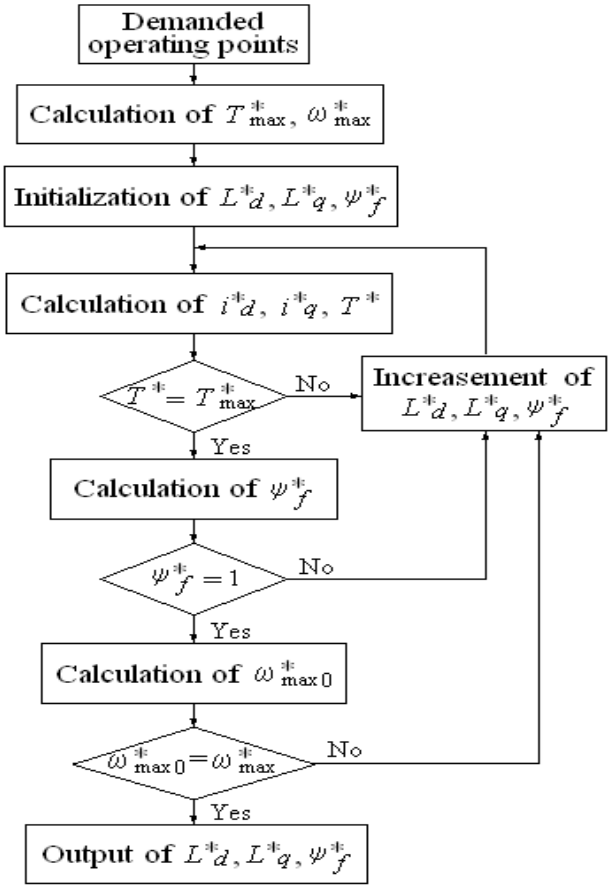

Fig. 9. Motor parameter surface and calculated output characteristic

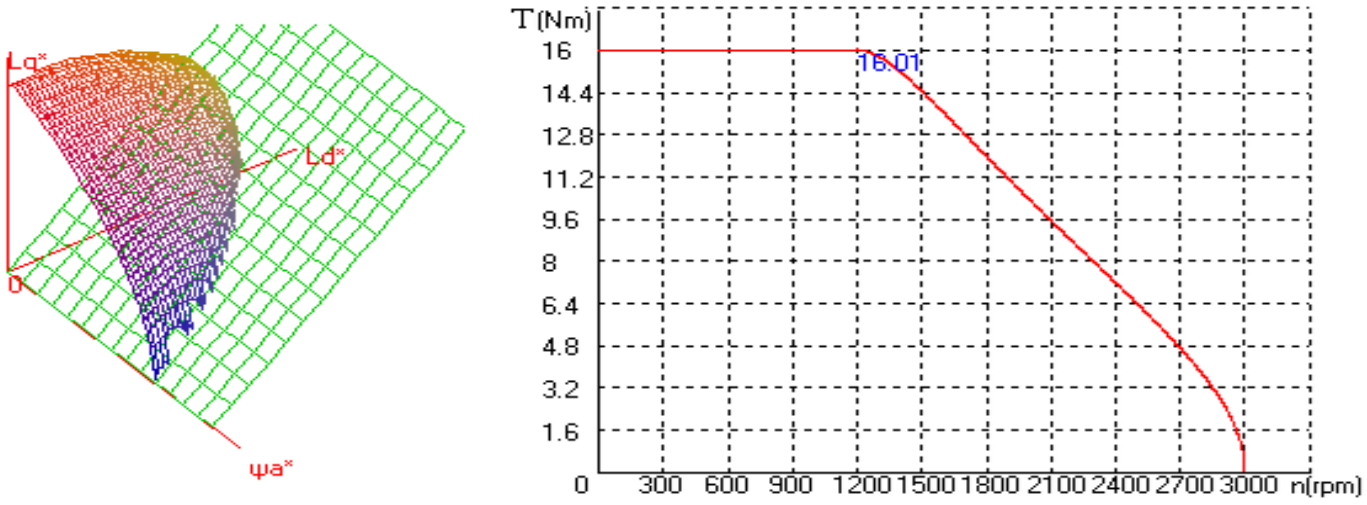

(a) 3-D parameter surface (b) Calculated output characteristic

It has taken the simulation with FEA (finite element analysis) as shown in Fig.10. The calculation results and FEA results are shown in Table 3.

An experimental prototype PMSM has been manufactured and tested for validation. Fig. 11 shows the torque-speed characteristics and power-speed characteristics from the measured values of the prototype motor.

Fig. 10. Flux density of PMSM design model

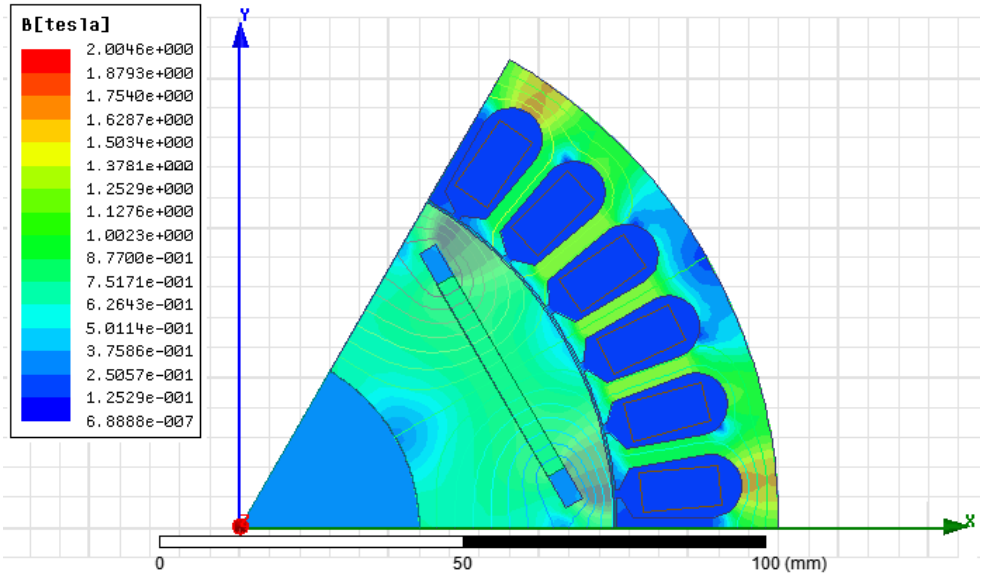

Table 3. Calculation result

Parameters	Relative value	Actual value	FEA result
d-axis inductance	0.47	0.606mH	0.597mH
q-axis inductance	0.62	0.799mH	0.813mH
armature flux linkage	0.87	0.054Wb	0.055Wb

Fig. 11. Output characteristics of the prototype PMSM

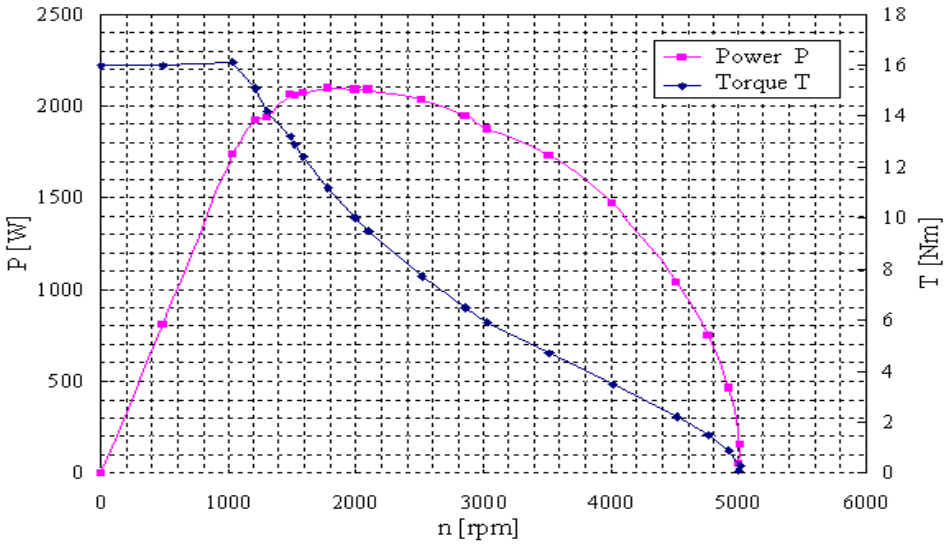

CONCLUSION

In this paper, we have studied the effects of the design parameters such as the d- and q-axis inductances and the magnetic flux linkage on the output characteristics of PMSM including the maximum torque and the maximum speed.

A design method for the parameters of the PMSM has been proposed to satisfy the desired torque-speed characteristics. The design parameters of a 16Nm IPMSM have been determined based on the proposed method. The mechanical characteristics calculated according to the design parameters satisfy the desired one with a relative error of about 0.63%.

A prototype PMSM with the determined parameters has been designed, simulated with FEA and manufactured for validation. The measured output characteristics were fully satisfied the desired one.

In future work, the effect of design parameters on the mechanical characteristics for either the maximum torque control or the maximum power control should be further investigated.

REFERENCES

1. C. López-Torres, A. G. Espinosa, J. Riba, and L. Romeral, “Design and optimization for vehicle driving cycle of rare-earth-free SynRM based on coupled lumped thermal and magnetic networks,” IEEE Transactions on Vehicle Technology, Vol. 67, No. 1, pp. 196–205, 2018
2. Chen. H, Demerdash. N.A.O, EL-Refaie. A.M, Guo. Y, Hua. W, “Investigation of a 3D-Magnetic Flux PMSM with High Torque Density for Electric Vehicles,” IEEE Transactions on Energy Conversion, Vol. 37, pp. 1442–1454, 2022.
3. F. David, K. Wolfgang, and K. Andreas, “Experimental Parameterization of a Design Model for Flatness-based Torque Control of a Saturated Surface-Mounted PMSM,” International Federation of Automatic Control (IFAC), pp. 575-582, 2016.
4. K. Yamano, S. Morimoto, M. Sanada, and Y. Inoue, “Design of Surface Permanent Magnet Synchronous

Motor Using Design Assist System for PMSM," IEEJ Journal of Industry Application, Vol. 6, No. 6, pp. 409-415, 2017.

5. L. Chen, J. Wang, P. Lazari, and X. Chen, "Optimizations of a permanent magnet machine targeting different driving cycles for electric vehicles," IEEE International Electric Machines and Drives Conference (IEMDC), pp. 855–862, 2013.
6. M. E. Beniakar, A. G. Sarigiannidis, P. E. Kakosimos, and A. G. Kladas, "Multiobjective evolutionary optimization of a surface mounted pm actuator with fractional slot winding for aerospace applications," IEEE Transactions on Magnetics, Vol. 50, No. 2, pp. 665–668, 2014.
7. M. Künzler, R. Pfüger, R. Lehmann, Q. Werner, "Dimensioning of a permanent magnet synchronous machine for electric vehicles according to performance and integration requirements," Automotive and Engine Technology, Vol. 7, pp. 97–104, 2022.
8. M. Sundaram, M. Anand, J. Chelladurai, P. Varunraj, S. J. Smith, S. Sharma, M. E. H. Assad, R. Alayi, "Design and FEM Analysis of High-Torque Power Density Permanent Magnet Synchronous Motor (PMSM) for Two-Wheeler E-Vehicle Applications," International Transactions on Electrical Energy Systems, Vol. 2022, Article ID 1217250, 2022.
9. N. Bernard, L. Dang, J. C. Olivier, N. Bracikowski, G. Wasselynck, and G. Berthiau, "Design Optimization of High-Speed PMSM for Electric Vehicles," Vehicle Power and Propulsion Conference (VPPC), 2015.
10. P. H. Nguyen, E. Hoang, M. Gabsi, L. Kobylanski, and D. Condamin, "Permanent magnet synchronous machines: Performances during driving cycles for a hybrid electric vehicle application," IEEE International Symposium on Industrial Electronics (ISIE), pp. 1432–1438, 2010.
11. R. R. Kumar and K. Alok, "Adoption of electric vehicle: a literature review and prospects for sustainability," Journal of Cleaner Production, Vol. 253, Article ID 119911, 2020.
12. R. T. Yadlapalli, A. Kotapati, R. Kandipati, and C. S. Koritala, "A review on energy efficient technologies for electric vehicle applications," Journal of Energy Storage, Vol. 50, Article ID 104212, 2022.
13. T. Ishikawa, K. Nakayama, N. Kurita, and F. P. Dawson, "Optimization of rotor topology in pm synchronous motors by genetic algorithm considering cluster of materials and cleaning procedure," IEEE Transactions on Magnetics, Vol. 50, No. 2, pp. 637–640, 2014.
14. T. Nakata, M. Sanada, S. Morimoto, and Y. Inoue, "Automatic design of IPMSMs using a genetic algorithm combined with the Coarse-Mesh FEM for enlarging the high-efficiency operation area," IEEE Transactions on Industrial Electronics, Vol. 64, No. 12, pp. 9721-9728, 2017.
15. V. Ruuskanen, J. Nerg, J. Pyrhönen, S. Ruotsalainen, and R. Kennel, "Drive cycle analysis of a permanent-magnet traction motor based on magneto static finite-element analysis," IEEE Transactions on Vehicle Technology, Vol. 64, No. 3, pp. 1249-1254, 2015
16. X. Li, Y. Zhao, "Design of High Energy Density Permanent Magnet Synchronous Motor", Proceedings of the 35th Chinese Control Conference, pp. 10232-10235, 2016.
17. Y. Gao, T. Yang, S. Bozhko, P. Wheeler, T. Dragicevic, C. Gerada, "Neural Network aided PMSM multi-objective design and optimization for more-electric aircraft applications," Chinese Journal of Aeronautics, Vol. 35, No.10, pp. 233-246, 2022.
18. Y. Hidaka, T. Sato, and H. Igarashi, "Topology optimization method based on on–off method and level set approach," IEEE Transactions on Magnetics, Vol. 50, No. 2, pp. 617–620, 2014.
19. Y. Okamoto, Y. Tominaga, S. Wakao, and S. Sato, "Topology optimization of rotor core combined with

identification of current phase angle in ipm motor using multistep genetic algorithm," IEEE Transactions on Magnetics, Vol. 50, No. 2, pp. 725–728, 2014.

20. Z. Shi, X. Sun, Y. Cai, X. Tian, and L. Chen, "Design optimisation of an outer-rotor permanent magnet synchronous hub motor for a low-speed campus patrol EV," IET Electric Power Applications, Vol. 14, No. 11, pp. 2111–2118, 2020.